Molecular Vision 2023; 29:87-101 <http://www.molvis.org/molvis/v29/87>
Received 15 November 2022 | Accepted 14 July 2023 | Published 16 July 2023

The impact of early RPE cell junction loss on VEGF, Ang-2, and TIMP secretion in vitro

Chase Paterson, Jamen Cannon, Elizabeth Vargis

Utah State University, Biological Engineering, Logan, UT

Purpose: The retinal pigment epithelium (RPE) is an important tissue for maintaining a healthy retina. Retinal pigment epithelial cells help regulate nutrient transport to photoreceptors and are heavily pigmented to prevent light scattering. These cells also have junction proteins to form monolayers. Monolayers are key players in pathologies such as age-related macular degeneration (AMD), a leading cause of vision loss in older adults. During AMD, RPE cell detachment can occur, resulting in a loss of junctions. Losing junctions can increase the expression of pro-angiogenic vascular endothelial growth factor (VEGF). This overexpression can cause abnormal blood vessel growth or angiogenesis in the retina. Age-related macular degeneration treatments target VEGF to slow angiogenesis progression. However, other proteins, such as angiopoietin-2 (Ang-2) and the tissue inhibitor of metalloproteinase-1 (TIMP-1), may also play important roles, making them potential targets for treatment. Controlling RPE junction formation will help elucidate the relationship between RPE cell detachment and additional angiogenic factor secretion, lead to more therapeutics, and increase the efficacy of current treatments.

Methods: Micropatterning was used to control the spatial arrangement of primary porcine RPE cells using polydimethylsiloxane (PDMS) stencils. Patterns were formed into PDMS stencils to mimic 10%, 25%, and 50% overall detachment of the RPE monolayer. Zonula-occludens-1 (ZO-1), Ang-2, and VEGF were visualized using immunocytochemical (ICC) staining. An enzyme-linked immunosorbent assay (ELISA) was used to quantify extracellular Ang-2, VEGF, TIMP-1, and TIMP-2 levels. A rod outer segment (OS) phagocytosis assay was performed to determine how RPE junction loss directly affects photoreceptor support.

Results: The growth of primary porcine RPE cells was successfully controlled using stencils. Morphological changes and a decrease in pigmentation were observed, showing a decline in barrier and light absorption functions as degeneration increased. One day after stencil removal, junction proteins were delocalized, and angiogenic factor secretions were correlated with increased levels of detachment. Secretion levels of Ang-2 and TIMP-1 were significantly increased, whereas VEGF and TIMP-2 concentrations were not as affected by varying levels of detachment. OS phagocytosis appeared lower in RPE cells when ZO-1 was affected.

Conclusions: These results suggest a correlation between loss of junctions, abnormal angiogenic protein secretion, and reduced OS phagocytosis. Furthermore, Ang-2 and TIMP-1 proteins might be beneficial targets for AMD treatments, and their roles in retinal diseases deserve further investigation.

The retina is a complex tissue responsible for capturing and transmitting light signals. The layers of the outer retina include photoreceptors, retinal pigment epithelium (RPE), Bruch's membrane, and vasculature known as the choroid (Figure 1A). These layers work together to maintain vision, and the RPE performs many functions to support photoreceptors and the choroid. RPE cells phagocytose photoreceptor outer segments (OS) to prevent toxin buildup and recycle crucial compounds for the vision cycle. They also secrete angiogenic factors, help regulate the extracellular matrix (ECM), and maintain a polarized monolayer with junctional proteins [1-5].

RPE cells form junctions to maintain healthy and uniform monolayers. Zonula occludens-1 (ZO-1) is an integral junction protein that helps link other junctional proteins to the cell cytoskeleton to maintain monolayer integrity [6]. There is a link between decreased ZO-1 and RPE cells developing epithelial mesenchymal transition phenotypes, which severely impact their ability to maintain retinal health [6,7]. Without these junctions, RPE cells are unable to support the other retinal layers. This lack of support can lead to diseases such as age-related macular degeneration (AMD) or diabetic retinopathy, in which vision becomes compromised [6-9].

Age-related macular degeneration is the leading cause of vision loss in older adults, and in 2019, it affected nearly 20 million people in the United States alone [10,11]. It is a progressive disease that is first characterized by lipid deposits called drusen that form posterior to the RPE (Figure 1B) [12-14]. Late AMD consists of two forms: atrophic (dry, Figure 1C) and exudative (wet, Figure 1D). Approximately 10% of patients with atrophic AMD develop more severe exudative AMD (BrightFocus Foundation). In exudative AMD, choroidal neovascularization (CNV) occurs, in which

Correspondence to: Elizabeth Vargis, Utah State University, Biological Engineering, 4105 Old Main Hill, Logan, UT 84321; Phone: (435) 797-0618; FAX: (435) 7971-248; email: vargis@usu.edu

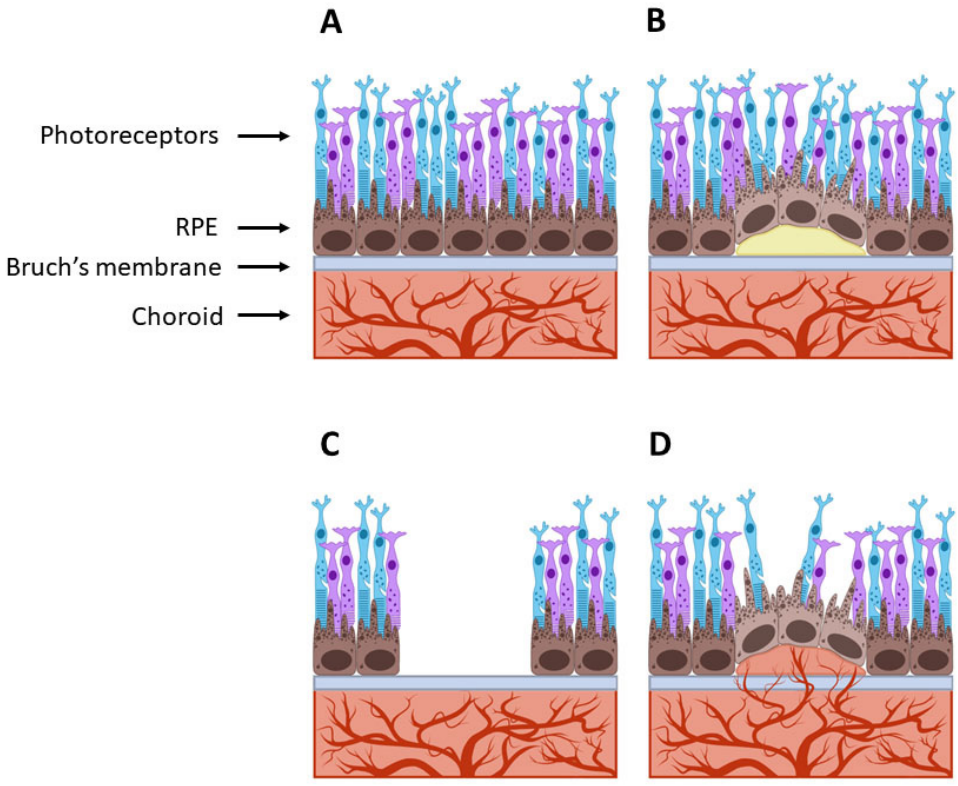

Figure 1. Diagrams of the retina. **A**: Healthy retina. **B**: Drusen formation, a hallmark of AMD. **C**: Atrophic late-stage AMD. **D**: Exudative late-stage AMD.

abnormal blood vessels grow and invade the retina, potentially leading to irreversible blindness [15,16].

While the specifics of AMD progression are not completely understood, the imbalanced secretion of angiogenic factors from the RPE plays a role. To help support the choroid, RPE cells secrete pro-angiogenic factors such as vascular endothelial growth factor (VEGF) and angiopoietin-2 (Ang-2) [17-19]. The regulated secretion of angiogenic factors is important in maintaining photoreceptor and choroidal health [20-22]. However, an increase in VEGF causes CNV [23-25]. Similarly, Ang-2 is upregulated in patients with exudative AMD and is correlated with disease severity [26]. While there are currently no treatments for atrophic AMD, the standard treatment for exudative AMD is anti-VEGF injections. However, some studies have shown that therapeutics targeting both VEGF and Ang-2 are more successful in suppressing CNV [27,28].

Although there is sufficient information on the role of angiogenic factors in AMD, the link between junction loss and angiogenic changes remains unclear. Junctional proteins, such as ZO-1, are likely to be affected early in the disease, such as when drusen begin to form. Understanding initial cell responses to junction disruption, such as how angiogenic factors are affected due to losing junctions, could provide more insight into the early stages of the disease and potentially new treatment options to prevent or delay impacts on visual acuity.

Other important aspects of AMD are changes in Bruch's membrane. Bruch's membrane thickens from the accumulation of lipids, the majority of which are secreted by the RPE [29]. However, improper ECM regulation also impacts the thickening of Bruch's membrane [30]. One way that RPE cells participate in ECM regulation is by secreting tissue inhibitors of metalloproteinases (TIMPs). These proteins help regulate metalloproteinases, and, in doing so, contribute to ECM proteolysis and wound repair, which are key elements of angiogenesis [31-33]. Different TIMP proteins have varied implications for retinal pathologies. For example, TIMP-1 is strongly upregulated in mouse retinal detachment and plays a role in angiogenesis [31,34]. However, TIMP-2 inhibits angiogenesis and helps stabilize new blood vessels [35,36].

One stimulus that might lead to the imbalance of angiogenic proteins is the loss of RPE junctions through cell–cell detachment or tears in the monolayer. This phenomenon can occur spontaneously during AMD or even during injections of anti-VEGF treatments [37-39]. Furthermore, during geographic atrophy, a hallmark of atrophic AMD, RPE cell contact is disrupted due to RPE cell death [40,41].

Unfortunately, the relationship between RPE cell junctions and angiogenic protein levels is not well understood. Previous work in our research group [42-45] showed an increase in VEGF when RPE cell detachment occurred, but more research is needed to elucidate further whether other proteins are affected.

Current methods for investigating RPE cell junctions include scratching assays, animal models, and genetic knockouts [6,42,46-49]. These techniques are often nonmimetic, expensive, or difficult to replicate. To overcome these challenges, we used micropatterning. Micropatterning consistently controls the spatial arrangement of cells and is appropriate for a variety of applications, such as in vitro tissue models, cell differentiation and migration analysis, and cell–cell interaction studies [42,50-53]. Many micropatterning techniques are available, including microcontact printing, microfluidic patterning, and stencil patterning [54]. Stencil patterning was chosen for this study because it does not require adhesion proteins for cell attachment, permits more complex shapes and arrangements, and can selectively and consistently control the detachment of cells grown in a monolayer.

In this work, stencils that mimicked AMD progression were generated to control the spatial arrangement of RPE cells and to cause different levels of detachment. These levels of detachment caused more cells to be removed and left larger gaps in the RPE monolayer as the stencil size increased. The stencils prevented RPE growth in 10%, 25%, and 50% of the overall growth area. These gaps in the monolayer provide less severe (10%) to extreme (50%) cases for what might occur in AMD as the disease progresses. The secretion of angiogenic and ECM factors was then analyzed to determine the downstream effects of RPE degeneration.

METHODS

Patterned wafer fabrication: The micropattern designs were based on geometries found in geographic atrophy [55,56] and scaled to prevent cell growth in 10%, 25%, and 50% of the overall growth area. The micropatterns were created and scaled using AutoCAD software. Photolithography was used to generate a patterned wafer. Briefly, a silicon wafer (University Wafer, South Boston, MA) was oxygen plasma treated for 1 min and spin coated with SU-8 2100 photoresist (Kayaku Advanced Materials, Westborough, MA), using a CEE® model 200X spin coater (Brewer Science, Rolla, MO) at the settings listed in Table 1. The coated wafer was placed on a hotplate for a prebake at 95 °C for 7 min and then 115 °C for 1 h. Afterwards, the wafer was exposed to ultraviolet light using a mask aligner (Midas System, Yuseong-gu, Daejeon, South Korea) for 8 s before immediately heating at 95 °C for 5 min and 115 °C for 25 min. The coated wafer was placed in a container with an SU-8 developer (Kayaku Advanced Materials, Westborough, MA) on an orbital shaker for 25 min at 32 RPM. The wafer was then sprayed with developer solution for 10 s, rinsed with isopropyl alcohol, and dried using a nitrogen blower.

Table 1. Spin coater settings for photoresist distribution during wafer fabrication.

Velocity (RPM)	Ramp (RPM)	Time (s)
500	100	10
1200	300	30

Mold and stencil creation: The wafer was oxygen plasma treated for 1 min and then silanized using 1H, 1H, 2H, 2H-perfluorooctyltrichlorosilane (Alfa Aesar, Haverhill, MA) for 1 h. Then, polydimethylsiloxane (PDMS, Sylgard 184, Dow Corning, Midland, MI) was mixed at a 10:1 ratio, poured directly over the patterned wafer, and vacuumed to remove air bubbles. The PDMS mold was cured at 50 °C overnight and then carefully removed using a scalpel. To facilitate stencil removal, the mold was silanized three times for 1 h each. Next, additional 10:1 PDMS was mixed, vacuumed, and poured directly onto the mold. Then, the excess PDMS was gently removed by scraping the mold with a glass slide. The mold was vacuumed for 30 min and then cured at 50 °C for 45 min. To minimize meniscus formation, additional PDMS was added to the partially cured stencils using a syringe, vacuumed for 15 min, and then cured overnight at 50 °C before the stencils were extracted from the mold using tweezers. The stencils were cleaned by sonication with 70% ethanol, followed by sonication with distilled water. The stencils were dried and then autoclaved for sterility before use in the cell culture.

Stencil verification: The fabricated stencils were measured using image stitching in ImageJ [57]. Images of each stencil were taken at 40× magnification and categorized by stencil size and image position. The images were then stitched into a composite image using ImageJ. The scale was set for each image based on the calibration obtained from the microscope at 1168 pixels/mm. Each stencil outline was traced three times, and measurements of the area and perimeter were taken and averaged. This process was repeated on three stencils of each size.

Primary RPE cell isolation: Primary RPE cells were isolated similarly to Farjood et al. [43]. Briefly, fresh porcine eyes were obtained from a local butcher shop. Exterior tissues were discarded, and the eyeballs were washed in 10%

povidone-iodine (Equate, Rogers, AR) before rinsing in cold PBS. Using tweezers, the eyes were placed on a sterile gauze and cut along the globe near the ora serrata. After discarding the vitreous, the eye cups were filled with cold PBS, and the neural retina was gently peeled away from the RPE using blunt tweezers. To eliminate excess neural retina, the eye cups were washed with cold PBS before filling with 0.25% trypsin containing 2.21 mM disodium ethylenediaminetetraacetic acid (EDTA; Corning Inc., Corning, NY) and incubated at 37 °C for 45 min. Retinal pigment epithelial cells were then collected using a combination of trituration and gentle brushing, utilizing a nylon paintbrush, and centrifuged at 250 RCF for 5 min. To help prevent clumping, the cells were suspended in media containing 100 µg/ml of DNase (Millipore Sigma, Burlington, MA) and incubated for 15 min. The cells were centrifuged again at 150 RCF for 5 min, and the supernatant was removed. Finally, the cells were seeded in a 6-well plate at a density of 2–3 eyes per well. The cells were fed Dulbecco's Modified Eagle Medium (DMEM; Corning Inc., Corning, NY), supplemented with 10% fetal bovine serum (FBS; VWR International, Radnor, PA), and 1% penicillin-streptomycin (Hyclone Laboratories Inc., Logan, UT) until confluency, when the concentration of FBS was dropped to 2% for culturing until experimentation.

RPE cell seeding and culture: The RPE cells were seeded at a density of 3×10^5 cells/cm^2 in 14 mm diameter glass microwells of 6-well plates (Cellvis, Mountain View, CA). The plates and stencils were oxygen plasma treated for 1 min separately. Then, the stencils were placed in the microwells, covered with cell media, and vacuumed for at least 50 min to remove air bubbles before the cells were added. The cells were allowed to attach for 24 h before the addition of extra media. The cells were grown in DMEM containing 10% FBS and 1% penicillin-streptomycin. On day 4, one day after confluency, the stencils were removed, and the cells were washed three times with Dulbecco's phosphate buffered saline (DPBS) and grown for 1 day before analysis. The cells were switched to 1% FBS media at the time of stencil removal. The growth media were changed every other day, and only passage 1 cultures were used.

Immunocytochemical (ICC) staining: Confocal microscopy and ICC staining were used to assess intracellular VEGF, Ang-2, and ZO-1. The VEGF and ZO-1 were stained with primary conjugated antibodies (Biorbyt, Cambridge, UK and Invitrogen, Waltham, MA) overnight at 4 °C. Ang-2 primary antibodies (Novus Biologicals, Littleton, CO) were stained with AF488 secondary antibodies (Invitrogen, Waltham, MA) for 1 h at room temperature. The nuclei were counterstained with NucBlue live cell stain (Thermo Fisher Scientific, Eugene, OR). An LSM-710 Carl Zeiss confocal microscope (Jena, Germany) was used to visualize the respective proteins. The dilutions for each antibody are listed in Table 2.

Table 2. Antibody dilutions and incubation times.

Antibody	Dilution	Incubation time
ZO-1	1	overnight
VEGF	1:400	overnight
Ang-2	1:1000	overnight
AF 488	2	1 h

Enzyme-linked immunosorbent assay (ELISA): Cell culture supernatants were collected 24 h after stencil removal, centrifuged at 300 RCF to remove debris, and frozen at −20 °C until use. To quantify the concentration of different angiogenic factors (Ang-2, TIMP-1, TIMP-2, and VEGF), a Q-Plex Human Angiogenesis kit (Quansys Biosciences, Logan, UT) was used according to the manufacturer's protocol and imaged using a Q-View Imager LS. Q-View software was used to analyze pixel intensity. The ELISA results were paired with the cell counts obtained with a Trypan blue exclusion assay.

Rod OS phagocytosis assay: Bovine rod outer segments (OS, InVision BioResources, Seattle, WA) were added to the cultures 1 day after stencil removal, at approximately 20 OS per cell. The RPE cells were challenged with OS for 4 h and then washed to remove unphagocytosed OS. The cells were fixed and stained with an anti-rhodopsin antibody and counterstained with the NucBlue live cell stain. Confocal microscopy was used to visualize the phagocytosed OS.

The OS were quantified by processing the fluorescent images using Fiji software [58]. Briefly, the upper threshold was set to 130 based on the control image (normal cell monolayer), and only particles larger than 2 µm^2 were counted to exclude artifacts. The outlines of the cell growth boundaries for the stencil images were manually drawn three times for each image to create regions of interest and to obtain the areas covered by cell growth. For the control image, a region of interest for each stencil type was overlayed, and the respective areas were used to calculate the number of OS per 100 µm^2.

Statistical analysis: A one-way ANOVA with Tukey post-hoc analysis was used to establish significance. A p-value < 0.05 was considered statistically significant.

RESULTS

Photolithography techniques generate mimetic and consistent micropatterned stencils: To verify that photolithography techniques generated micropatterned stencils with expected area and perimeter parameters, and therefore desired levels of RPE detachment, fabricated stencils were analyzed using ImageJ. As shown in Table 3, there was minimal variety in the sizes of the measured areas and perimeters of the stencil.

Micropatterned stencils control the growth of the RPE monolayer, and detachment causes abnormal cell morphology: The cells were visualized with bright-field microscopy before and after stencil removal to determine whether the stencils controlled the growth of the RPE cell monolayer (Figure 2). Immediately after stencil removal, the RPE monolayer maintained the desired shape of the stencil. One day later, the cells on the edge of the stenciled area exhibited abnormal morphological changes (Figure 2D). The cells were more elongated and less pigmented than cells that had not experienced the loss of a neighbor.

Detachment results in scattered ZO-1 localization: The ZO-1 protein expression was visualized using ICC and imaged with a confocal microscope (Figure 3) to analyze the effect of detachment on the junctions of the RPE cells. In the control, in which cells grew in the microwells without a stencil, the cells exhibited the expected intercellular ZO-1 expression (Figure 3B). The cells growing on the edge of the stenciled area had scattered and delocalized ZO-1 expression (Figure 3F), indicating that the cells were unable to form consistent junctions.

Changes in angiogenic expression vary with ZO-1 delocalization: To analyze if RPE cells that experienced detachment of a neighboring cell exhibited different localization of pro-angiogenic proteins VEGF and Ang-2, ICC imaging was used (Figure 4 and Figure 5). While there were cells in which VEGF expression appeared higher (Figure 4, arrows), the cells near the edge did not display consistent changes in VEGF expression. The Ang-2 expression was higher in cells that had disrupted junctional proteins (Figure 5F–T) than in the control (Figure 5A–E). Similar Ang-2 results were seen at a lower magnification (data not shown). An ELISA was also used to quantify how cell–cell detachment affected the expression of these proteins.

Angiogenic protein secretion changes with increasing levels of detachment: The expressions of various proteins were quantified to determine how varying levels of detachment and subsequent RPE degeneration play a role in AMD progression. The concentrations of Ang-2, TIMP-1, TIMP-2, and VEGF were obtained from the cell culture media 1 day after stencil removal (Figure 6). The Ang-2 and TIMP-1 levels increased statistically significantly as the levels of detachment increased. However, TIMP-2 and VEGF secretions were not significantly affected by detachment.

Table 3. Micropatterned stencil measurements.

Stencil size	Predicted area [mm^2]	Measured area [mm^2]	Predicted perimeter [mm]	Measured perimeter [mm]
10%	15.35	15.70±0.46	22.40	22.75±0.28
25%	38.50	38.67±0.68	35.48	35.68±0.35
50%	76.97	75.45±3.36	50.16	49.51±0.62

Rod OS phagocytosis decreases during RPE cell degeneration: A rod outer segment (OS) phagocytosis assay was performed to analyze how RPE degradation caused by cell-cell detachment affects crucial physiological functions. One day after stencil removal, the cells were challenged with a rod OS and then imaged with a confocal microscope (Figure 7). Under normal conditions, the RPE cells appeared to engulf the OS evenly (Figure 7B) and had a 0.09 ± 12E-4 OS per 100 µm^2. However, the wells where detachment occurred had noticeably fewer OS present on the edge where the cells had compromised junctions (Figure 7E,H,K). The cells grown in response to 10%, 25%, and 50% stencils had 0.11 ± 1.7E-4, 0.07 ± 1.5E-4, and 0.03 ± 6.7E-5 OS per 100 µm^2, respectively.

DISCUSSION

The role of RPE degeneration in AMD is not fully understood. One instance of RPE degeneration observed during AMD is geographic atrophy when cell–cell contact is lost. When RPE cell detachment occurs in AMD, junctions are compromised in the remaining cells. While geographic atrophy expands over time, a model that shows what occurs in a short timeframe after RPE cells initially respond to detachment would be beneficial. The goals of this manuscript are to better understand how the initial loss of junctions leads to increased degeneration of the RPE monolayer and to elucidate possible early treatment targets.

To evaluate whether RPE junction integrity affects angiogenesis and the ECM, stencils of varying sizes (Table 3) were used to mimic increasing levels of detachment and control RPE cell growth. In this micropatterned model, RPE cells grew around the specifically designed stencil (Figure 2). When the stencil was removed, a layer of cells was removed (Appendix 1), and the RPE junctions of the remaining cells were compromised. These stencils eliminate the need for chemical disruption of junctions or adhesion proteins. Additionally, this in vitro micropatterned technique provides

inexpensive and rapid experimentation that is limited to in vivo methods.

First, it was important to model RPE cell–cell detachment to see how it might play a role in AMD progression through the disruption of junctions and overexpression of angiogenic factors. Junctions are important in maintaining an RPE cell monolayer, which is essential to the function of the RPE [6]. To validate that this micropatterned method replicates what happens during aging or disease, ZO-1 proteins were visualized using ICC. Normally, ZO-1 proteins remain on cell boundaries to link other junctional proteins to the cytoskeleton [59,60]. Under the control conditions, ZO-1 expression remained exclusively on the cell boundaries (Figure 3B). Conversely, RPE cells responding to stencil removal had scattered, abnormal ZO-1 (Figure 3F), which may be an indicator of losing polarity and undergoing epithelial mesenchymal transition (EMT). Epithelial mesenchymal transition has been implicated in retinal diseases, such as AMD. These results are similar to those of Georgiadis et al., who found that RPE cells with downregulated ZO-1 lost typical epithelial monolayer characteristics and appeared flattened and elongated in vivo [6]. While it is known that the loss of junctions is a characteristic of EMT [7,61-63], the correlation between junction loss and angiogenic secretion needs to be investigated.

Typically, RPE cells secrete angiogenic factors, such as VEGF and Ang-2, to support the health of the choroid [17-19]. An imbalance of angiogenic factors is a major contributor to AMD [64-66]. Even so, less is known about what initially leads to this imbalance. To determine whether the localization of angiogenic proteins was affected by RPE degradation caused by the loss of intercellular junctions, VEGF, and

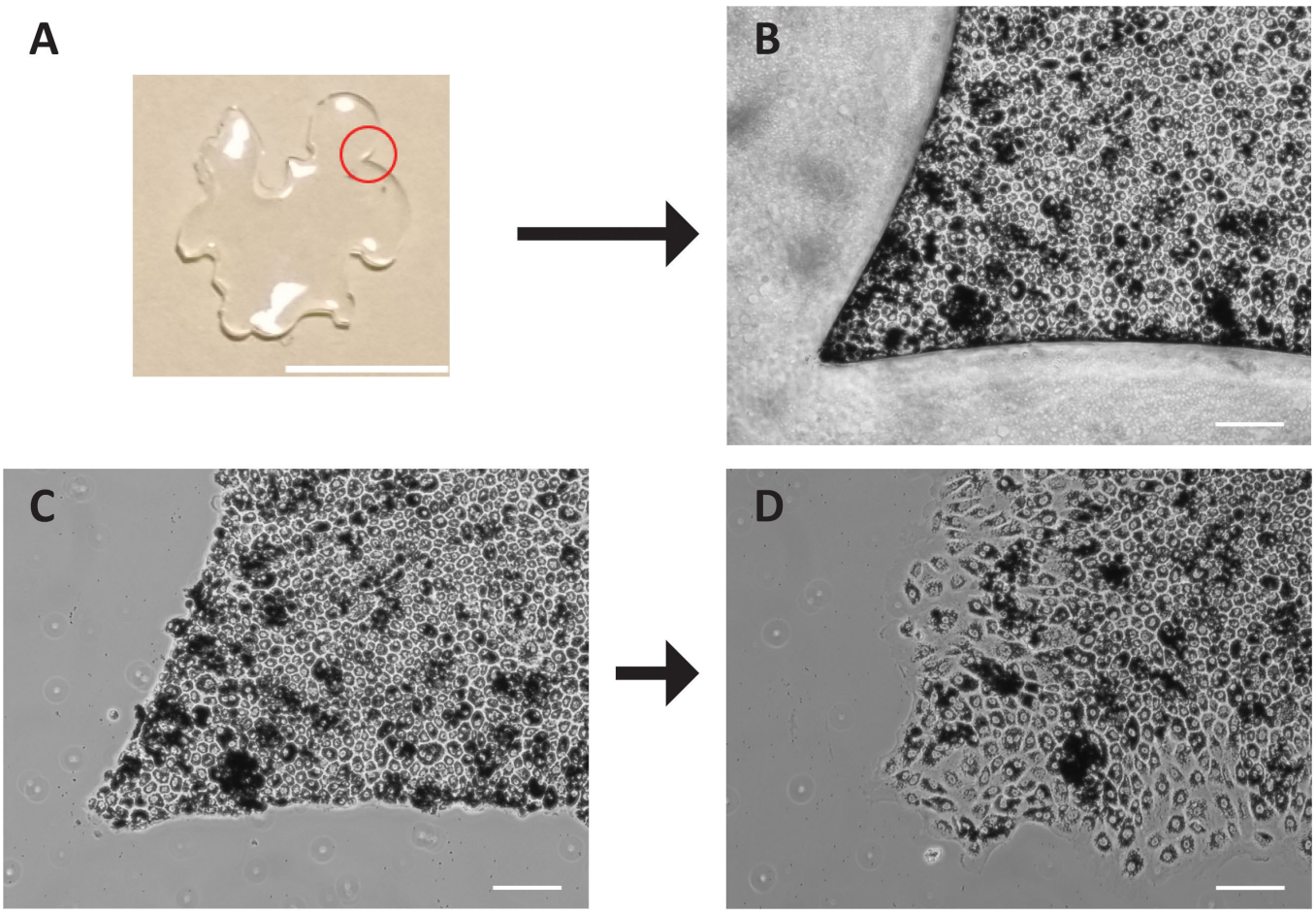

Figure 2. Images showing an overview of RPE cell growth before and after stencil removal. A: Image of a micropatterned stencil to mimic 25% detachment. B: Bright-field images of the stencil effectively controlling RPE cell growth. C: Immediately after the stencil was removed, the monolayer maintained the shape of the stencil. D: One day after stencil removal, the cells grew into the empty space and experienced morphological changes and pigment loss. Scale bars: 5 mm (A) and 100 µm (B–D).

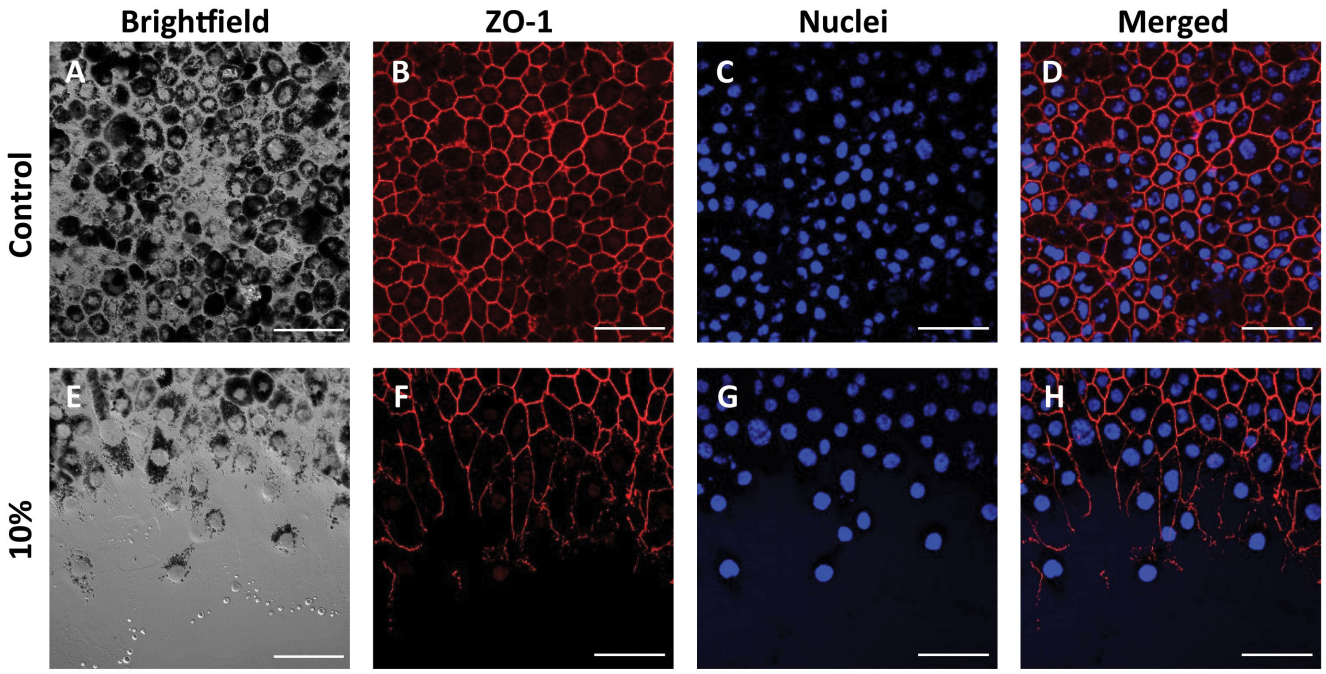

Figure 3. Visualization of tight junction protein ZO-1 (red) and nuclei (blue) 1 day after stencil removal. A–D: Cells grown under normal conditions exhibited the expected intercellular ZO-1 expression. E–H: Cells that experienced the removal of neighbors due to a 10% stencil had fragmented ZO-1 localization. Scale bars: 50 µm.

Ang-2 proteins were visualized using ICC (Figure 4 and Figure 5). The VEGF expression appeared to be higher in some cells growing on the edge of a stenciled area (Figure 4, arrows). However, the increased expression was not consistent, implying that VEGF expression was not substantially affected soon after detachment. Different results were seen with Ang-2, as cells that lost their neighbors had consistently higher expression than cells in the control wells (Figure 5).

In addition to VEGF and Ang-2, RPE cells secrete TIMPs to maintain the surrounding ECM [31-33]. While lipid deposition plays a major role in drusen formation (Figure 1B), unregulated ECM and RPE dysfunction are also believed to contribute [14]. An increase in TIMP-1 can lead to ECM buildup and fibrosis [67]. Additionally, higher levels of TIMP-1 are seen in patients experiencing geographic atrophy [68]. Tissue inhibitors of metalloproteinase proteins also play roles in angiogenesis, cell growth, and apoptosis [69,70]. Previous studies have shown that TIMP-1 has anti-angiogenic properties [71], while others have indicated the opposite [72]. Lastly, research has indicated that TIMP proteins, junctions, and pro-angiogenic factors all play key roles in barrier functions. One study found a correlation between decreased ZO-1 and TIMP levels in impaired blood–brain barrier function [73]. Another study found decreased ZO-1 and increased Ang-2 when the blood–retinal barrier was damaged [74]. With their role in ECM regulation, quantifying the secretion of TIMP proteins is crucial. An ELISA was used to quantify TIMP-1 and TIMP-2 as well as the Ang-2 and VEGF proteins to better understand how the loss of RPE junctions might contribute to ECM remodeling or angiogenesis.

One day after stencil removal, Ang-2 and TIMP-1 secretion increased significantly with detachment (Figure 6), indicating a correlation with junction loss. Our results demonstrate that RPE cells respond to losing their neighboring cells by secreting more Ang-2, which has been shown to be upregulated in CNV-derived RPE cells [75]. By controlling RPE cell–cell detachment, we also found that the remaining RPE cells overexpressed TIMP-1. Similarly, Kwok et al. found that TIMP-1 secretion was significantly increased in immortalized adult RPE cells (ARPE-19) cells 24 h after laser exposure [76]. Therefore, TIMP-1 overexpression could play a role in AMD progression through fibrotic and inflammatory pathways and likely influences drusen formation. These results indicate that Ang-2 and TIMP-1 may be potential therapeutic targets and merit further investigation into their role in the progression of AMD.

Intriguingly, VEGF secretion was not immediately affected by increasing levels of detachment (Figure 6). These results imply that VEGF might play a larger role in later RPE cell responses to detachment or might have time-dependent

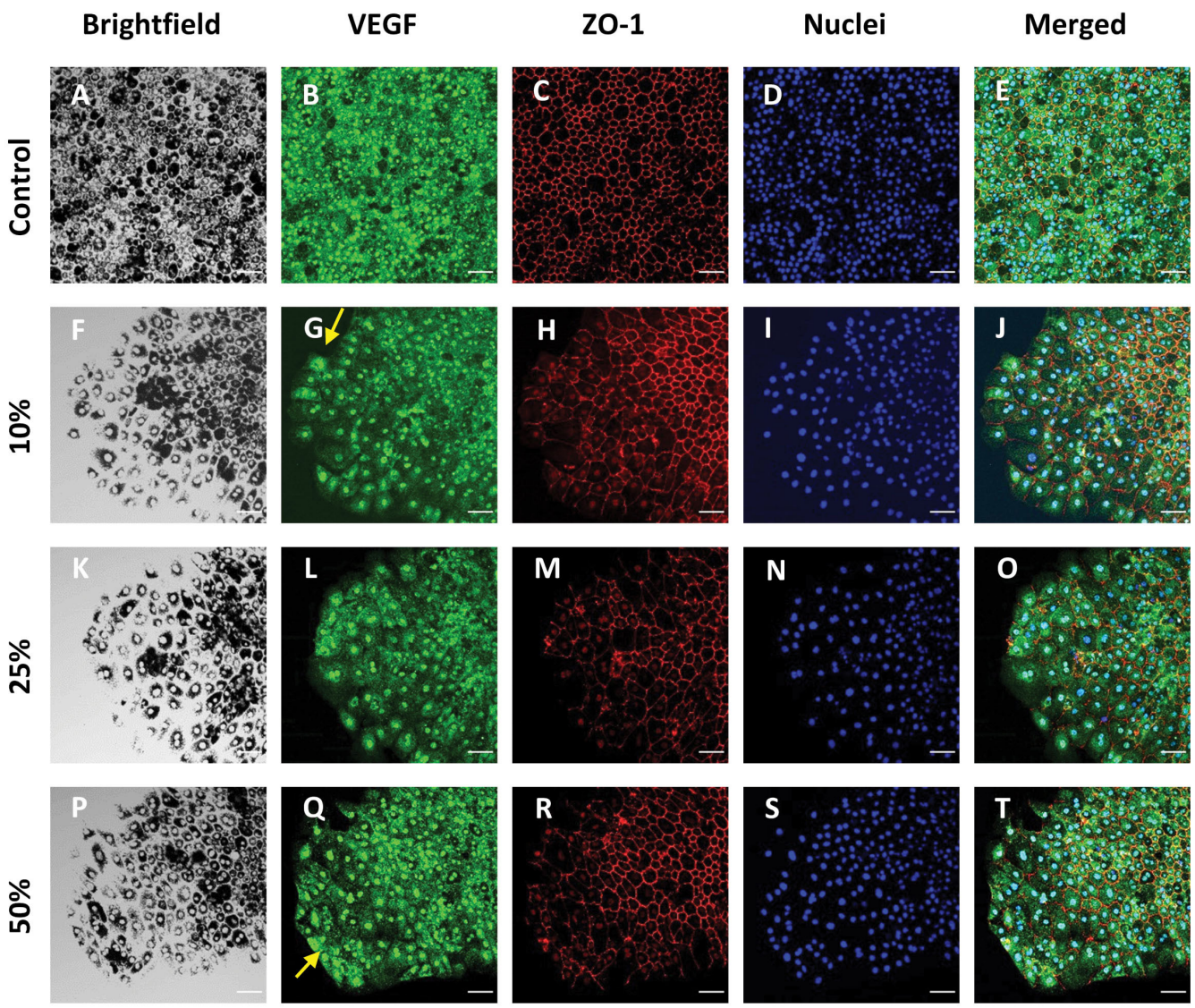

Figure 4. Images of VEGF (green), ZO-1 (red), and nuclei (blue) 1 day after the stencils were removed. A–E: Cells grown under normal conditions had uniform VEGF expression (B) and normal ZO-1 localization (C). F–T: Cells that experienced intercellular junction removal appeared to have a higher expression of VEGF in some locations (arrows) but not consistently across edges of detachment. These cells also had more scattered ZO-1 (H, M, and R). Scale bars: 50 µm.

changes in expression. Wang et al. found an increase in VEGF gene expression 3 h after disrupting RPE cell adhesion and junctions through calcium chelation or reduction [48]. However, the expression decreased gradually within 24 h. Unlike the results found in this study, Wang et al. showed no change in TIMP-1 through calcium-mediated cell dissociation. Additionally, it is speculated that gene expression could be directly affected by cellular calcium concentration, which could explain the differences in the results [48].

Tissue inhibitors of metalloproteinase-2, which has anti-angiogenic properties, was unaffected [35,70]. In contrast, Zhang et al. found that sodium iodate suppressed TIMP-2 in ARPE-19 cells, but that TIMP-1 remained unaffected. These changes also occurred alongside reduced expression of ZO-1 [77]. Although the exact role of TIMPs in AMD is unknown, our results elucidate how RPE detachment affects these proteins early on and how they might affect the progression of AMD. However, more research must be done to better understand the role of TIMPs in AMD and other retinal diseases.

A crucial function of RPE cells is to phagocytose photoreceptor OS. OS are shed daily to prevent the accumulation of toxic compounds in photoreceptors. After phagocytosis,

the key components of the visual cycle are recycled back into the photoreceptors [5,78]. Dysfunction of OS phagocytosis by the RPE has been linked to numerous retinal diseases and is believed to contribute to AMD [79-81]. To understand how the disruption of RPE junctions might directly affect photoreceptor support, an OS phagocytosis assay was performed. Under normal conditions, OS were seen throughout the culture (Figure 7B). However, degenerated RPE cells growing near the edge of the micropatterned areas (Figure 7E,H,K) appeared to have fewer OS. When quantified, the cells grown with the 10% stencil had the most OS per area. However, the cells grown with the 25% and 50% stencils had fewer OS than both the 10% stencil and the control cells, indicating that, at high enough levels of detachment, the numbers of OS decrease. These results indicate a correlation between junction loss and the ability to phagocytose OS. Without proper OS phagocytosis, waste accrues between retinal layers, encouraging inflammation and drusen formation [82,83]. Moreover, key compounds, such as 11-*cis*-retinal, are not transported by the RPE and could lead to decreased light perception by photoreceptors [1]. Therefore, it is likely that RPE cell–cell detachment quickly leads to an adverse impact on photoreceptor health and contributes to waste accumulation in the retina.

Although the outcomes of this research helped to develop a better understanding of certain aspects of retinal diseases,

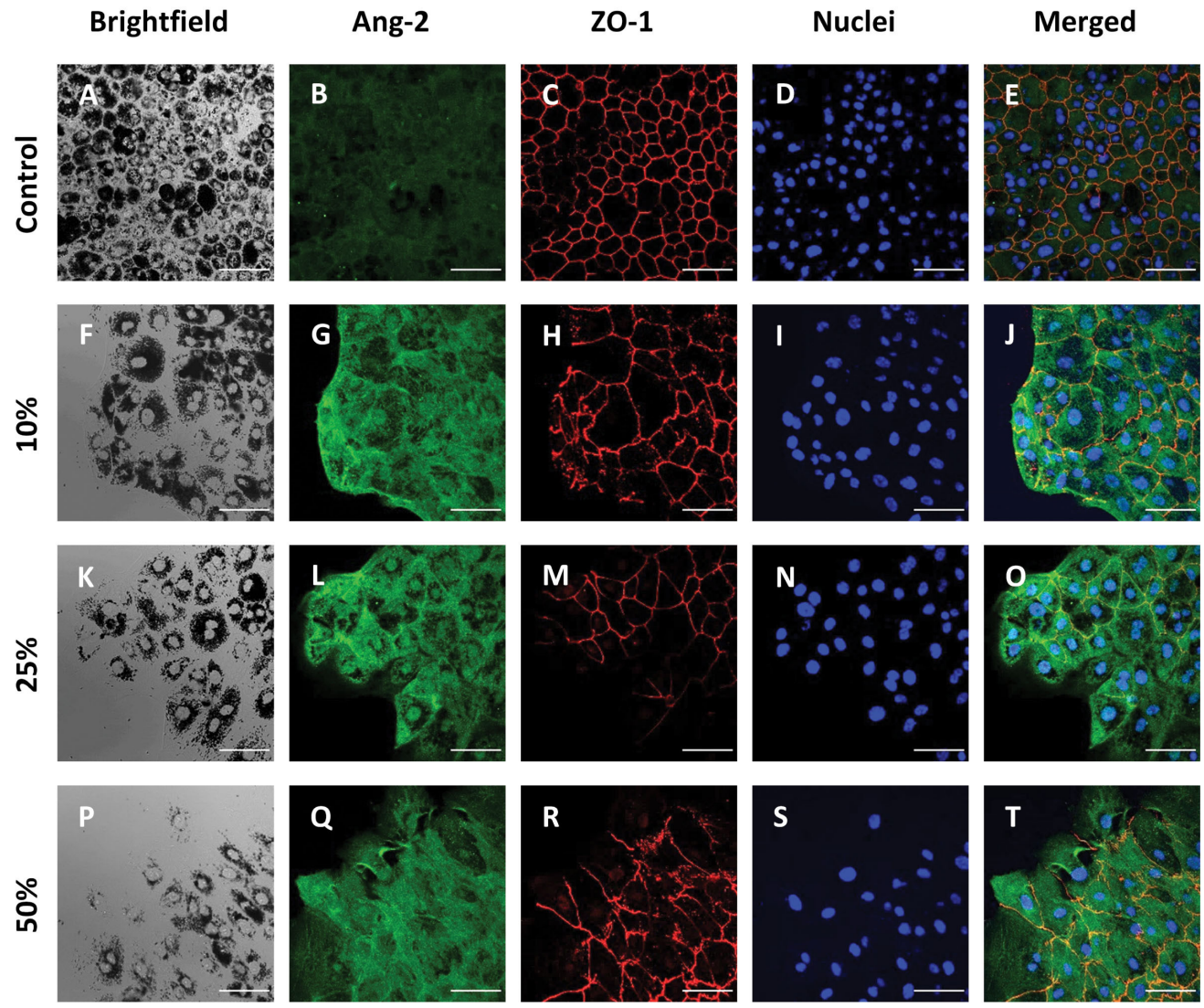

Figure 5. Visualization of Ang-2 (green), ZO-1 (red), and nuclei (blue) 1 day after the stencils were removed. A–E: Cells grown under normal conditions exhibited less Ang-2 expression and more intercellular ZO-1 localization. F–T: Cells that responded to stencil removal appeared to have increased Ang-2 expression. These cells also had more scattered ZO-1 localization (H, M, and R). Scale bars: 50 µm.

there were some unexpected results. Specifically, there were areas where ZO-1 appeared disrupted in the control and did not fully enclose the cell boundaries (Figure 3). However, these areas corresponded to more heavily pigmented cells, which may have hindered fluorescence [84]. While VEGF was not significantly affected in our experiments, it is possible that the change in VEGF across 10%, 25%, and 50% detachment could be minimal with early RPE detachment but increase after chronic RPE degeneration. Additionally, these results further show that early degeneration of the RPE has a large impact on Ang-2 expression, which verifies the use of VEGF-Ang-2 combinatorial treatments, such as VABYSMO, which was approved for exudative AMD treatment in January 2022. Additionally, the binding of Ang-2 sensitizes

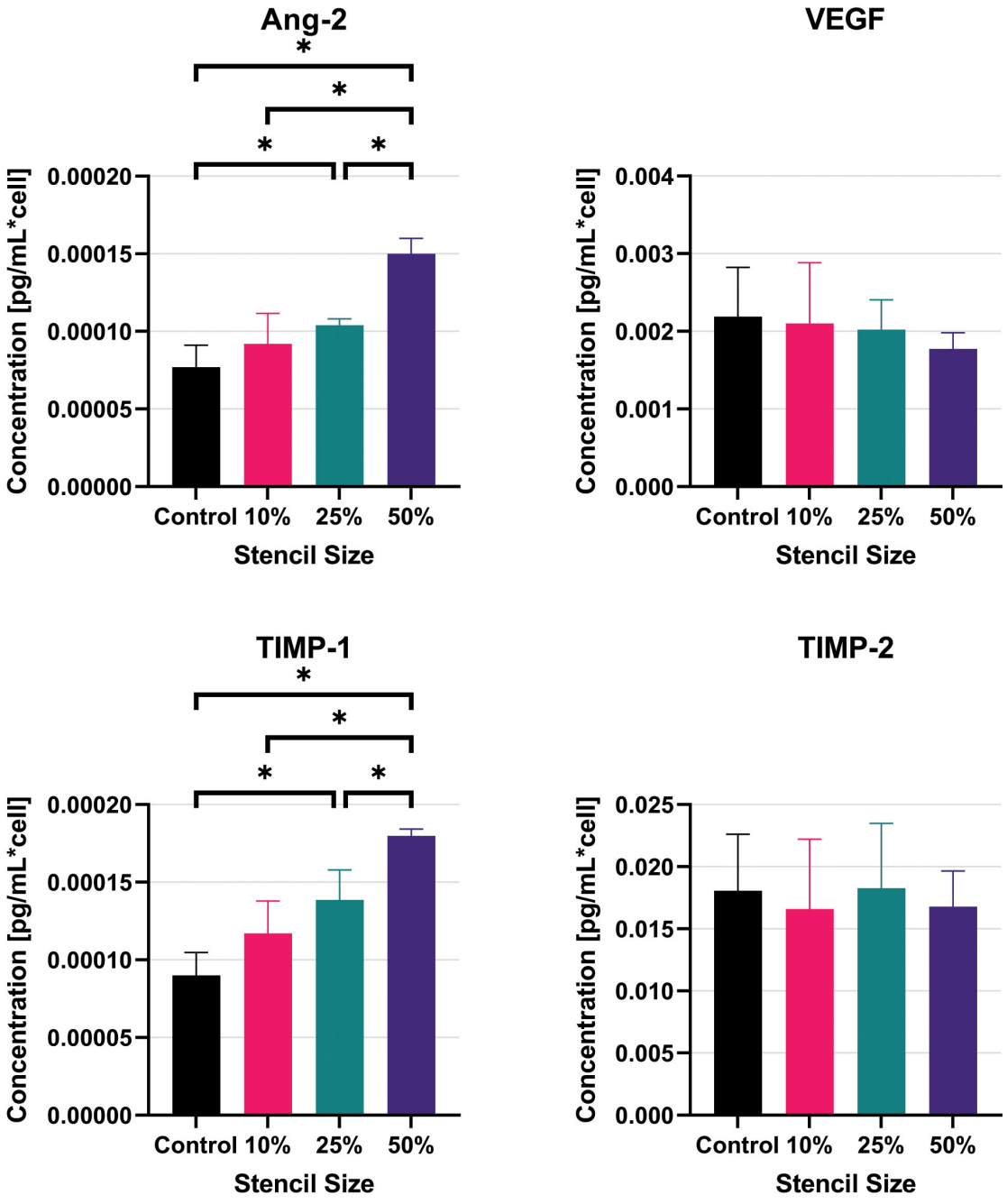

Figure 6. Mean concentrations of Ang-2, VEGF, TIMP-1, and TIMP-2 proteins in cell media 1 day after stencil removal. Error bars represent standard deviations. * *p*-value < 0.05. Control (*n* = 7), 10% (*n* = 4), 25% (*n* = 4), 50% (*n* = 4).

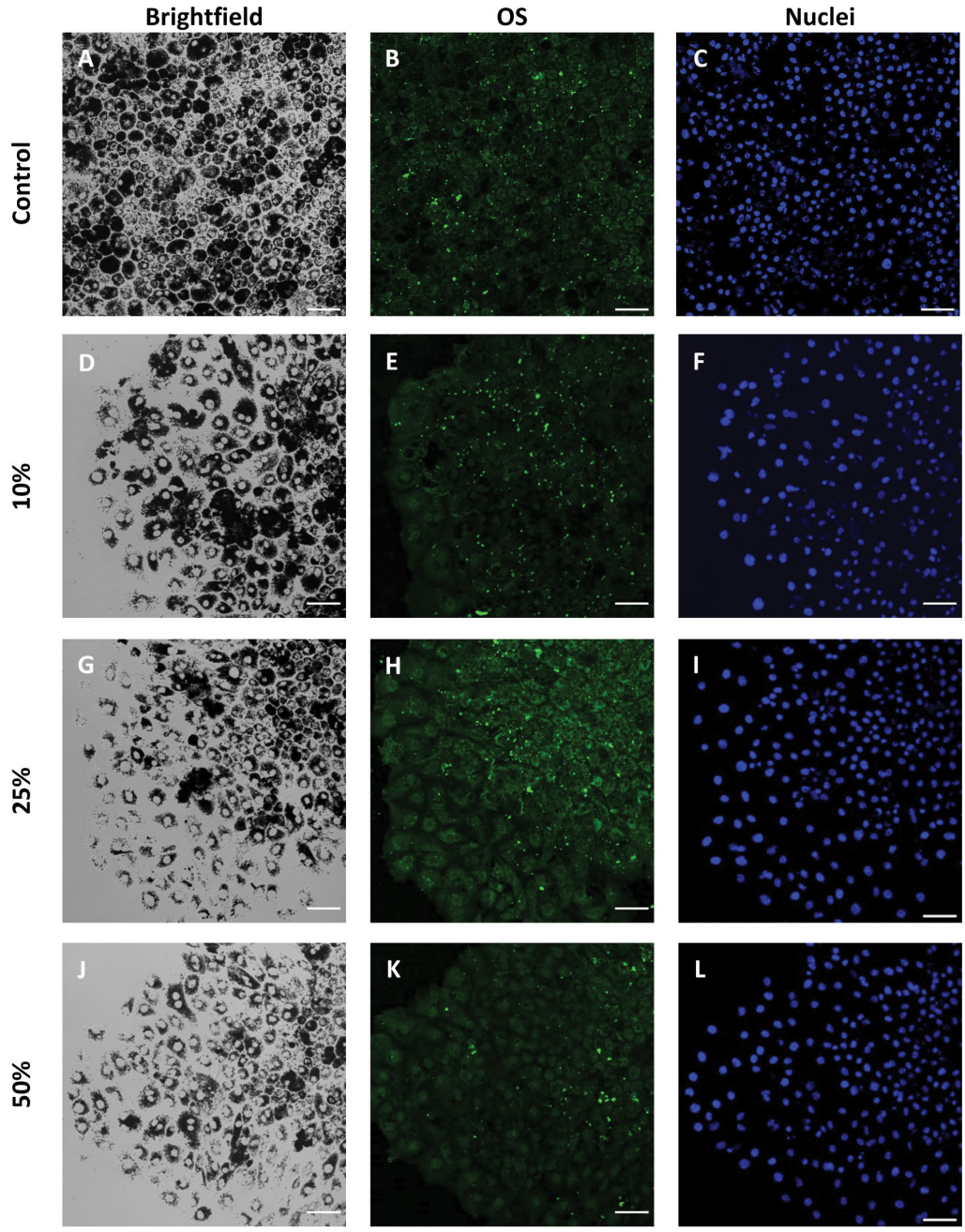

Figure 7. Rod outer segment (OS) phagocytosis 1 day after stencil removal. OS (bright green) were seen in all samples, but fewer appeared near the edge where junctional proteins were affected. Cells grown without a stencil that did not experience detachment were used as controls. Scale bars: 50 µm.

endothelial cells to VEGF [19], indicating that perhaps Ang-2 plays a more important role in the early cascade of CNV, which leads to retinal destabilization.

It is important to note that inflammation is another key player in AMD [85]. Not only is inflammation believed to contribute to drusen formation [86,87], it also affects junction proteins [88,89]. While the micropattern methods in this paper do not instigate junction loss through chemical means that directly cause inflammation, the physical detachment could potentially lead to increased inflammatory factors, or represent what occurs after an increase in inflammation. A model that combines physical detachment and the overexpression

of inflammation agents, such as oxidants, may further help elucidate how RPE cells respond in multifactorial diseases.

In conclusion, abnormal RPE cell behavior caused by cell–cell detachment led to a significant increase in Ang-2 and TIMP-1 secretion in a micropatterned model of AMD. However, VEGF and TIMP-2 were not significantly affected. The loss of RPE junctions correlated with changes in angiogenic factors and a decrease in OS phagocytosis. These results offer insight into new therapeutic options and further clarify the process behind AMD and other diseases, such as diabetic retinopathy. Future work will explain how other proteins might play a role in the progression of retinal pathologies.

APPENDIX 1. IMAGES SHOWING SUCCESSFUL DETACHMENT OF RPE CELLS USING A MICROPATTERNED STENCIL.

To access the data, click or select the words "Appendix 1." A: Bright-field image of cells that had been growing next to the stencil and have detached when the stencil was removed. B: Fluorescent image showing nuclei of removed cells. Scale bar: 100 µm.

ACKNOWLEDGMENTS

The authors would like to thank Dillon Weatherston and Teren Teeples for help with cell culture, Emilee Rickabaugh for retinal schematics, and Thomas Harris for paper edits. This work was supported by a National Eye Institute of the National Institutes of Health Grant R15EY028732.

REFERENCES

1. Strauss O. The Retinal Pigment Epithelium in Visual Function. Physiol Rev 2005; 85:845-81. [PMID: 15987797].
2. Mazzoni F, Safa H, Finnemann SC. Understanding photoreceptor outer segment phagocytosis: Use and utility of RPE cells in culture. Exp Eye Res 2014; 0:51-60. [PMID: 24780752].
3. Kolko M, Vosborg F, Henriksen UL, Hasan-Olive MM, Diget EH, Vohra R, Gurubaran IRS, Gjedde A, Mariga ST, Skytt DM, Utheim TP, Storm-Mathisen J, Bergersen LH. Lactate Transport and Receptor Actions in Retina: Potential Roles in Retinal Function and Disease. Neurochem Res 2016; 41:1229-36. [PMID: 26677077].
4. Sparrow JR, Hicks D, Hamel CP. The Retinal Pigment Epithelium in Health and Disease. Curr Mol Med 2010; 10:802-23. [PMID: 21091424].
5. Kocaoglu OP, Liu Z, Zhang F, Kurokawa K, Jonnal RS, Miller DT. Photoreceptor disc shedding in the living human eye. Biomed Opt Express 2016; 7:4554-68. [PMID: 27895995].
6. Georgiadis A, Tschernutter M, Bainbridge JWB, Balaggan KS, Mowat F, West EL, Munro PMG, Thrasher AJ, Matter K, Balda MS, Ali RR. The Tight Junction Associated Signalling Proteins ZO-1 and ZONAB Regulate Retinal Pigment Epithelium Homeostasis in Mice. PLoS One 2010; 5:e15730[PMID: 21209887].
7. Zhou M, Geathers JS, Grillo SL, Weber SR, Wang W, Zhao Y, Sundstrom JM. Role of Epithelial-Mesenchymal Transition in Retinal Pigment Epithelium Dysfunction. Front Cell Dev Biol 2020; 8:501-[PMID: 32671066].
8. Naylor A, Hopkins A, Hudson N, Campbell M. Tight Junctions of the Outer Blood Retina Barrier. Int J Mol Sci 2020; 21:211-[PMID: 31892251].
9. Yang S, Zhou J, Li D. Functions and Diseases of the Retinal Pigment Epithelium. Front Pharmacol 2021; 12:727870-[PMID: 34393803].
10. Ambati J, Fowler BJ. Mechanisms of age-related macular degeneration. Neuron 2012; 75:26-39. [PMID: 22794258].
11. Rein DB, Wittenborn JS, Burke-Conte Z, Gulia R, Robalik T, Ehrlich JR, Lundeen EA, Flaxman AD. Prevalence of Age-Related Macular Degeneration in the US in 2019. JAMA Ophthalmol 2022; 140:1202-1208. [PMID: 36326752].
12. Hageman GS, Luthert PJ, Victor Chong NH, Johnson LV, Anderson DH, Mullins RF. An Integrated Hypothesis That Considers Drusen as Biomarkers of Immune-Mediated Processes at the RPE-Bruch's Membrane Interface in Aging and Age-Related Macular Degeneration. Prog Retin Eye Res 2001; 20:705-32. [PMID: 11587915].
13. Kanduri S. Current understanding of Age-related macular degeneration. Int J Retina. 2020;3.
14. Zhang X, Sivaprasad S. Drusen and pachydrusen: the definition, pathogenesis, and clinical significance. Eye (Lond) 2021; 35:121-33. [PMID: 33208847].
15. Yin H, Fang X, Ma J, Chen M, Yang Y, Guo S, Chen Z, Su Z, Feng L, Ye P, Wu F, Yin J. Idiopathic Choroidal Neovascularization: Intraocular Inflammatory Cytokines and the Effect of Intravitreal Ranibizumab Treatment. Sci Rep 2016; 6:31880-[PMID: 27558944].
16. Bhutto I, Lutty G. Understanding age-related macular degeneration (AMD): Relationships between the photoreceptor/retinal pigment epithelium/Bruch's membrane/choriocapillaris complex. Mol Aspects Med 2012; 33:295-317. [PMID: 22542780].
17. Marneros AG, Fan J, Yokoyama Y, Gerber HP, Ferrara N, Crouch RK, Olsen BR. Vascular Endothelial Growth Factor Expression in the Retinal Pigment Epithelium Is Essential for Choriocapillaris Development and Visual Function. Am J Pathol 2005; 167:1451-9. [PMID: 16251428].
18. Peters S, Cree IA, Alexander R, Turowski P, Ockrim Z, Patel J, Boyd SR, Joussen AM, Ziemssen F, Hykin PG, Moss SE. Angiopoietin modulation of vascular endothelial growth factor: Effects on retinal endothelial cell permeability. Cytokine 2007; 40:144-50. [PMID: 17959386].

19. Joussen AM, Ricci F, Paris LP, Korn C, Quezada-Ruiz C, Zarbin M. Angiopoietin/Tie2 signalling and its role in retinal and choroidal vascular diseases: a review of preclinical data. Eye (Lond) 2021; 35:1305-16. [PMID: 33564135].

20. Ohno-Matsui K, Morita I, Tombran-Tink J, Mrazek D, Onodera M, Uetama T, Hayano M. Murota S itsu, Mochizuki M. Novel mechanism for age-related macular degeneration: An equilibrium shift between the angiogenesis factors VEGF and PEDF. J Cell Physiol 2001; 189:323-33. [PMID: 11748590].

21. Sonoda S, Sreekumar PG, Kase S, Spee C, Ryan SJ, Kannan R, Hinton DR. Attainment of polarity promotes growth factor secretion by retinal pigment epithelial cells: Relevance to age-related macular degeneration. Aging 2009; 2:28-42. [PMID: 20228934].

22. Farjo KM. Ma J xing. The potential of nanomedicine therapies to treat neovascular disease in the retina. J Angiogenes Res 2010; 2:21-[PMID: 20932321].

23. Marneros AG. Increased VEGF-A promotes multiple distinct aging diseases of the eye through shared pathomechanisms. EMBO Mol Med 2016; 8:208-31. [PMID: 26912740].

24. Saishin Y, Saishin Y, Takahashi K, Silva RL, Hylton D, Rudge JS, Wiegand SJ. Campochiaro PA. VEGF-TRAPR1R2 suppresses choroidal neovascularization and VEGF-induced breakdown of the blood–retinal barrier. J Cell Physiol 2003; 195:241-8. [PMID: 12652651].

25. Kwak N, Okamoto N, Wood JM, Campochiaro PA. VEGF Is Major Stimulator in Model of Choroidal Neovascularization. Invest Ophthalmol Vis Sci 2000; 41:3158-64. [PMID: 10967078].

26. Ng DS, Yip YW, Bakthavatsalam M, Chen LJ, Ng TK, Lai TY, Pang CP, Brelén ME. Elevated angiopoietin 2 in aqueous of patients with neovascular age related macular degeneration correlates with disease severity at presentation. Sci Rep 2017; 7:45081-[PMID: 28345626].

27. Foxton RH, Uhles S, Grüner S, Revelant F, Ullmer C. Efficacy of simultaneous VEGF-A/ANG-2 neutralization in suppressing spontaneous choroidal neovascularization. EMBO Mol Med 2019; 11:e10204-[PMID: 31040126].

28. Sahni J, Patel SS, Dugel PU, Khanani AM, Jhaveri CD, Wykoff CC, Hershberger VS, Pauly-Evers M, Sadikhov S, Szczesny P, Schwab D, Nogoceke E, Osborne A, Weikert R, Fauser S. Simultaneous Inhibition of Angiopoietin-2 and Vascular Endothelial Growth Factor-A with Faricimab in Diabetic Macular Edema: BOULEVARD Phase 2 Randomized Trial. Ophthalmology 2019; 126:1155-70. [PMID: 30905643].

29. Curcio CA, Johnson M, Rudolf M, Huang JD. The oil spill in ageing Bruch membrane. Br J Ophthalmol 2011; 95:1638-45. [PMID: 21890786].

30. Hussain AA, Lee Y, Zhang JJ, Marshall J. Disturbed Matrix Metalloproteinase Activity of Bruch's Membrane in Age-Related Macular Degeneration. Invest Ophthalmol Vis Sci 2011; 52:4459-66. [PMID: 21498613].

31. Aplin AC, Zhu WH, Fogel E, Nicosia RF. Vascular regression and survival are differentially regulated by MT1-MMP and TIMPs in the aortic ring model of angiogenesis. Am J Physiol Cell Physiol 2009; 297:C471-80. [PMID: 19494241].

32. García-Onrubia L, Valentín-Bravo Fco J, Coco-Martin RM, González-Sarmiento R, Pastor JC, Usategui-Martín R, Pastor-Idoate S. Matrix Metalloproteinases in Age-Related Macular Degeneration (AMD). Int J Mol Sci 2020; 21:5934-[PMID: 32824762].

33. Egea V, Zahler S, Rieth N, Neth P, Popp T, Kehe K, Jochum M, Ries C. Tissue inhibitor of metalloproteinase-1 (TIMP-1) regulates mesenchymal stem cells through let-7f microRNA and Wnt/β-catenin signaling. Proc Natl Acad Sci USA 2012; 109:E309-16. [PMID: 22223664].

34. Kim B, Abdel-Rahman MH, Wang T, Pouly S, Mahmoud AM, Cebulla CM. Retinal MMP-12, MMP-13, TIMP-1, and TIMP-2 Expression in Murine Experimental Retinal Detachment. Invest Ophthalmol Vis Sci 2014; 55:2031-40. [PMID: 24526442].

35. Brew K, Nagase H. The tissue inhibitors of metalloproteinases (TIMPs): An ancient family with structural and functional diversity. Biochim Biophys Acta BBAMol Cell Res 2010; 1803:55-71. [PMID: 20080133].

36. Nikolov A, Popovski N, Hristova I. Collagenases MMP-1, MMP-13, and Tissue Inhibitors TIMP-1, TIMP-2: Their Role in Healthy and Complicated Pregnancy and Potential as Preeclampsia Biomarkers—A Brief Review. Appl Sci. 2020; 10:7731-.

37. Bakri SJ, Patel SP. Retinal pigment epithelial tear following intravitreal bevacizumab. Eye (Lond) 2007; 21:424-5. [PMID: 17187026].

38. Yeo JH, Marcus S, Murphy RP. Retinal pigment epithelial tears. Patterns and prognosis. Ophthalmology 1988; 95:8-13. [PMID: 2449643].

39. Leon PE, Saviano S, Zanei A, Pastore MR, Guaglione E, Mangogna A, Tognetto D. Spontaneous or secondary to intravitreal injections of anti-angiogenic agents retinal pigment epithelial tears in age-related macular degeneration. Int J Ophthalmol 2014; 7:681-5. [PMID: 25161943].

40. Hanus J, Zhang H, Wang Z, Liu Q, Zhou Q, Wang S. Induction of necrotic cell death by oxidative stress in retinal pigment epithelial cells. Cell Death Dis 2013; 4:e965-[PMID: 24336085].

41. Liang FQ, Godley BF. Oxidative stress-induced mitochondrial DNA damage in human retinal pigment epithelial cells: a possible mechanism for RPE aging and age-related macular degeneration. Exp Eye Res 2003; 76:397-403. [PMID: 12634104].

42. Farjood F, Vargis E. Physical disruption of cell–cell contact induces VEGF expression in RPE cells. Mol Vis 2017; 23:431-46. [PMID: 28761317].

43. Farjood F, Ahmadpour A, Ostvar S, Vargis E. Acute mechanical stress in primary porcine RPE cells induces angiogenic factor expression and in vitro angiogenesis. J Biol Eng 2020; 14:13-[PMID: 32355505].

44. Vargis E, Peterson CB, Morrell-Falvey JL, Retterer ST, Collier CP. The effect of retinal pigment epithelial cell patch size on growth factor expression. Biomaterials 2014; 04:3999-4004. .

45. Farjood F, Vargis E. Novel devices for studying acute and chronic mechanical stress in retinal pigment epithelial cells. Lab Chip 2018; 18:3413-24. [PMID: 30328441].

46. Klettner A, Brinkmann A, Winkelmann K, Käckenmeister T, Hildebrandt J, Roider J. Effect of long-term inflammation on viability and function of RPE cells. Exp Eye Res 2020; 200:108214-[PMID: 32898511].

47. Lv D, Chen D, Wang Z, Cui Z, Ma JH, Ji S, Chen J, Tang S. COL10A1 is a novel factor in the development of choroidal neovascularization. Microvasc Res 2022; 139:104239-[PMID: 34520774].

48. Wang XF, Cui JZ, Prasad SS, Matsubara JA. Altered Gene Expression of Angiogenic Factors Induced by Calcium-Mediated Dissociation of Retinal Pigment Epithelial Cells. Invest Ophthalmol Vis Sci 2005; 46:1508-15. [PMID: 15790923].

49. Ikeda Y, Yonemitsu Y, Onimaru M, Nakano T, Miyazaki M. Kohno R ichiro, Nakagawa K, Ueno A, Sueishi K, Ishibashi T. The regulation of vascular endothelial growth factors (VEGF-A, -C, and -D) expression in the retinal pigment epithelium. Exp Eye Res 2006; 83:1031-40. [PMID: 16842779].

50. Otsuka H, Sasaki K, Okimura S, Nagamura M, Nakasone Y. Micropatterned co-culture of hepatocyte spheroids layered on non-parenchymal cells to understand heterotypic cellular interactions. Sci Technol Adv Mater 2013; 14:065003-[PMID: 27877623].

51. Théry M. Micropatterning as a tool to decipher cell morphogenesis and functions. J Cell Sci 2010; 123:4201-13. [PMID: 21123618].

52. Song W, Lu H, Kawazoe N, Chen G. Adipogenic Differentiation of Individual Mesenchymal Stem Cell on Different Geometric Micropatterns. Langmuir 2011; 27:6155-62. [PMID: 21486006].

53. Sun Q, Liu C, Bai X, Huo B. Cell–substrate traction force regulates the fusion of osteoclast precursors through cell–cell interaction. Biomech Model Mechanobiol 2020; 19:481-92. [PMID: 31529292].

54. Liu WW, Chen ZL, Jiang XY. Methods for Cell Micropatterning on Two-Dimensional Surfaces and Their Applications in Biology. Chin J Anal Chem 2009; 37:943-9. .

55. Fleckenstein M, Mitchell P, Freund KB, Sadda S, Holz FG, Brittain C, Henry EC, Ferrara D. The Progression of Geographic Atrophy Secondary to Age-Related Macular Degeneration. Ophthalmology 2018; 125:369-90. [PMID: 29110945].

56. Sadda SR, Chakravarthy U, Birch DG, Staurenghi G, Henry EC, Brittain C. Clinical Endpoints for the Study of Geographic Atrophy Secondary to Age-Related Macular Degeneration. Retina 2016; 36:1806-22. [PMID: 27652913].

57. Preibisch S, Saalfeld S, Tomancak P. Globally optimal stitching of tiled 3D microscopic image acquisitions. Bioinformatics 2009; 25:1463-5. [PMID: 19346324].

58. Schindelin J, Arganda-Carreras I, Frise E, Kaynig V, Longair M, Pietzsch T, Preibisch S, Rueden C, Saalfeld S, Schmid B, Tinevez JY, White DJ, Hartenstein V, Eliceiri K, Tomancak P, Cardona A. Fiji - an Open Source platform for biological image analysis. Nat Methods 2012; 9:[PMID: 22743772].

59. Xu HZ, Song Z, Fu S, Zhu M, Le YZ. RPE barrier breakdown in diabetic retinopathy: seeing is believing. J Ocul Biol Dis Infor 2011; 4:83-92. [PMID: 23275801].

60. Förster C. Tight junctions and the modulation of barrier function in disease. Histochem Cell Biol 2008; 130:55-70. [PMID: 18415116].

61. Kalluri R, Weinberg RA. The basics of epithelial-mesenchymal transition. J Clin Invest 2009; 119:1420-8. [PMID: 19487818].

62. Yang J, Antin P, Berx G, Blanpain C, Brabletz T, Bronner M, Campbell K, Cano A, Casanova J, Christofori G, Dedhar S, Derynck R, Ford HL, Fuxe J, García de Herreros A, Goodall GJ, Hadjantonakis AK, Huang RYJ, Kalcheim C, Kalluri R, Kang Y, Khew-Goodall Y, Levine H, Liu J, Longmore GD, Mani SA, Massagué J, Mayor R, McClay D, Mostov KE, Newgreen DF, Nieto MA, Puisieux A, Runyan R, Savagner P, Stanger B, Stemmler MP, Takahashi Y, Takeichi M, Theveneau E, Thiery JP, Thompson EW, Weinberg RA, Williams ED, Xing J, Zhou BP, Sheng G. Guidelines and definitions for research on epithelial–mesenchymal transition. Nat Rev Mol Cell Biol 2020; 21:341-52. [PMID: 32300252].

63. Shu DY, Butcher E, Saint-Geniez M. EMT and EndMT: Emerging Roles in Age-Related Macular Degeneration. Int J Mol Sci 2020; 21:4271-[PMID: 32560057].

64. Gao G, Li Y, Zhang D, Gee S, Crosson C. Ma J xing. Unbalanced expression of VEGF and PEDF in ischemia-induced retinal neovascularization. FEBS Lett 2001; 489:270-6. [PMID: 11165263].

65. Tombran-Tink J. PEDF in Angiogenic Eye Diseases. Curr Mol Med 2010; 10:267-78. [PMID: 20236057].

66. Spilsbury K, Garrett KL, Shen WY, Constable IJ, Rakoczy PE. Overexpression of Vascular Endothelial Growth Factor (VEGF) in the Retinal Pigment Epithelium Leads to the Development of Choroidal Neovascularization. Am J Pathol 2000; 157:135-44. [PMID: 10880384].

67. Ramos de Carvalho JE, Verwoert MT, Vogels IMC, Reits EA, Van Noorden CJF, Klaassen I, Schlingemann RO. Involvement of the ubiquitin-proteasome system in the expression of extracellular matrix genes in retinal pigment epithelial cells. Biochem Biophys Rep. 2018; 13:83-92. [PMID: 29387813].

68. Krogh Nielsen M, Subhi Y, Rue Molbech C, Nilsson LL, Nissen MH, Sørensen TL. Imbalances in tissue inhibitors of metalloproteinases differentiate choroidal neovascularization from geographic atrophy. Acta Ophthalmol (Copenh) 2019; 97:84-90. [PMID: 30288950].

69. Quintero-Fabián S, Arreola R, Becerril-Villanueva E, Torres-Romero JC, Arana-Argáez V, Lara-Riegos J, Ramírez-Camacho MA, Alvarez-Sánchez ME. Role of Matrix Metalloproteinases in Angiogenesis and Cancer. Front Oncol 2019; 9:1370

70. Seo DW, Li H, Guedez L, Wingfield PT, Diaz T, Salloum R. Wei B yang, Stetler-Stevenson WG. TIMP-2 Mediated Inhibition of Angiogenesis: An MMP-Independent Mechanism. Cell 2003; 114:171-80. [PMID: 12887919].

71. Reed MJ. Inhibition of TIMP1 enhances angiogenesis in vivo and cell migration in vitro. Microvasc Res 2003; 65:9-17. [PMID: 12535866].

72. Yamada E, Tobe T, Yamada H, Okamoto N, Zack DJ, Werb Z, Soloway PD, Campochiaro PA. TIMP-1 promotes VEGF-induced neovascularization in the retina. Histol Histopathol 2001; 16:87-97. [PMID: 11193216].

73. Li Z, Mo N, Li L, Cao Y, Wang W, Liang Y, Deng H, Xing R, Yang L, Ni C, Chui D, Guo X. Surgery-Induced Hippocampal Angiotensin II Elevation Causes Blood-Brain Barrier Disruption via MMP/TIMP in Aged Rats. Front Cell Neurosci 2016; 10:105-[PMID: 27199659].

74. Guo J, Xiao F, Ren W, Zhu Y, Du Q, Li Q, Li X. Circular Ribonucleic Acid circFTO Promotes Angiogenesis and Impairs Blood–Retinal Barrier Via Targeting the miR-128–3p/Thioredoxin Interacting Protein Axis in Diabetic Retinopathy. Front Mol Biosci 2021; 8:685466-[PMID: 34422901].

75. Martin G, Schlunck G, Hansen LL, Agostini HT. Differential expression of angioregulatory factors in normal and CNV-derived human retinal pigment epithelium. Graefes Arch Clin Exp Ophthalmol 2004; 242:321-6. [PMID: 14722782].

76. Kwok AKH, Lai TYY, Yam HF, Pang CP. TIMP-1 production in human retinal pigment epithelial cells after laser exposure. Yan Ke Xue Bao. 2005; 21:31-7. [PMID: 17162914].

77. Zhang XY, Ng TK, Brelén ME, Wu D, Wang JX, Chan KP, Yung JSY, Cao D, Wang Y, Zhang S, Chan SO, Pang CP. Continuous exposure to non-lethal doses of sodium iodate induces retinal pigment epithelial cell dysfunction. Sci Rep 2016; 6:37279-[PMID: 27849035].

78. Kim SY. Retinal phagocytes in age-related macular degeneration. Macrophage. 2015; 2:e698-[PMID: 26052551].

79. Van Soest S, Westerveld A, De Jong PTVM, Bleeker-Wagemakers EM, Bergen AAB. Retinitis Pigmentosa: Defined From a Molecular Point of View. Surv Ophthalmol 1999; 43:321-34. [PMID: 10025514].

80. Sun K, Cai H, Priore LVD. Bruch's Membrane Aging Decreases Phagocytosis of Outer Segments by Retinal Pigment Epithelium. Invest Ophthalmol Vis Sci 2005; 46:4165-.

81. Li W. Phagocyte dysfunction, tissue aging and degeneration. Ageing Res Rev 2013; 12:1005-12. [PMID: 23748186].

82. Jiang M, Esteve-Rudd J, Lopes VS, Diemer T, Lillo C, Rump A, Williams DS. Microtubule motors transport phagosomes in the RPE, and lack of KLC1 leads to AMD-like pathogenesis. J Cell Biol 2015; 210:595-611. [PMID: 26261180].

83. Kwon W, Freeman SA. Phagocytosis by the Retinal Pigment Epithelium: Recognition, Resolution, Recycling. Front Immunol 2020; 11:604205-[PMID: 33281830].

84. Orchard GE, Calonje E. The Effect of Melanin Bleaching on Immunohistochemical Staining in Heavily Pigmented Melanocytic Neoplasms. Am J Dermatopathol 1998; 20:357-61. [PMID: 9700373].

85. Kauppinen A, Paterno JJ, Blasiak J, Salminen A, Kaarniranta K. Inflammation and its role in age-related macular degeneration. Cell Mol Life Sci 2016; 73:1765-86. [PMID: 26852158].

86. Anderson DH, Mullins RF, Hageman GS, Johnson LV. A role for local inflammation in the formation of drusen in the aging eye. Am J Ophthalmol 2002; 134:411-31. [PMID: 12208254].

87. Johnson LV, Forest DL, Banna CD, Radeke CM, Maloney MA, Hu J, Spencer CN, Walker AM, Tsie MS, Bok D, Radeke MJ, Anderson DH. Cell culture model that mimics drusen formation and triggers complement activation associated with age-related macular degeneration. Proc Natl Acad Sci USA 2011; 108:18277-82. [PMID: 21969589].

88. Bäsler K, Brandner JM. Tight junctions in skin inflammation. Pflüg Arch - Eur J Physiol 2017; 469:3-14. [PMID: 27853878].

89. Edelblum KL, Turner JR. The Tight Junction in Inflammatory Disease: Communication Breakdown. Curr Opin Pharmacol 2009; 9:715-20. [PMID: 19632896].

Articles are provided courtesy of Emory University and the Zhongshan Ophthalmic Center, Sun Yat-sen University, P.R. China. The print version of this article was created on 16 July 2023. This reflects all typographical corrections and errata to the article through that date. Details of any changes may be found in the online version of the article.